NORGES TEKNISK-NATURVITENSKAPELIGE UNIVERSITET

Uncertainty in Seismic Inversion for Reservoir Characterization

by

Alfhild Lien Eide, Henning Omre and Bjørn Ursin

PREPRINT

STATISTICS NO. 10/1999

NORWEGIAN UNIVERSITY OF SCIENCE AND TECHNOLOGY

TRONDHEIM, NORWAY

This report has URL http://www.math.ntnu.no/preprint/statistics/1999/S10-1999.ps

Alfhild Lien Eide has homepage: http://www.math.ntnu.no/~aeide

E-mail: aeide@math.ntnu.no

Address: Department of Mathematical Sciences, Norwegian University of Science and Technology,

N-7491 Trondheim, Norway.

Uncertainty in Seismic Inversion for Reservoir Characterization

Alfhild Lien Eide, Henning Omre and Bjørn Ursin*
Department of Mathematical Sciences,
Norwegian University of Science and Technology,
N-7491 Trondheim, Norway
omre@stat.ntnu.no

April 21, 1999

Abstract

Seismic inversion for reservoir characterization is a spatial, multivariate, ill-posed inverse problem. A Bayesian framework is used to determine a posterior model. Focus is on sampling from this posterior, which is complicated due to the high dimensionality of the problem, non-linearity in the likelihoods and complex conditioning. A sequential sampling algorithm can be defined under relatively weak assumptions. Samples of reservoir porosity and the wavelet parameter in the seismic model, are generated. Assessment of uncertainty in seismic inversion will make it possible to define more efficient data acquisition and depletion strategies for petroleum reservoirs. The methodology is demonstrated on data from the Troll Field in the North Sea.

Keywords: Spatial statistics, geostatistics, Bayesian model, Gaussian field.

*Department of Petroleum Engineering and Applied Geophysics, Norwegian University of Science and Technology, N-7491 Trondheim, Norway

1 Introduction

Important decisions in the petroleum industry are based on information from seismic data, and the processing of these data constitutes one of the most computer demanding tasks worldwide. Seismic data originate from acoustic pulses generated on the earth's surface and recording of the reflection from the earth's interior. The processing of these data consists of many parts, and one important aspect is inversion of the seismic signal into geologically meaningful variables. In the current paper inversion of seismic amplitudes into spatially varying porosities will be considered. Porosity is crucial for determining the volumetrics of groundwater and hydrocarbon reservoirs. Moreover, porosity is usually related to permeability, which is a fluid flow characteristic and hence is important when planning the depletion of these reservoirs. In order to forecast production, the reservoir characteristics must be used as input to a fluid flow simulator represented by a set of highly non-linear differential equations. Considering the importance of the problem, surprisingly few papers in the statistical literature can be found on the subject.

Seismic inversion is a spatial, multivariate, ill-posed inverse problem, and phrasing the problem in a Bayesian setting seems natural. The focus is not on obtaining a maximum aposteriori (MAP) solution, but rather on sampling from the posterior probability density function (pdf) for later to make production forecasts with uncertainty assessments. The problem has many similarities with meteorological forecasting, medical imaging and satellite imaging. One crucial characteristic of our problem, often overlooked in other applications, is that the observations are collected by different devices. Some observations are fairly exact measurements in wells drilled through the reservoir, other observations are indirectly obtained through non-linear transfer functions as seismic data. This requires physically based assessment of the likelihood models. A framework for this in reservoir evaluation is presented in Omre & Tjelmeland (1997).

In Tarantola (1987), the seismic inverse problem is cast in a Bayesian setting, but no spatial model is used. Bortoli, Alabert, Haas & Journel (1993) and Haas & Dubrule (1994) introduce a spatial model, but sample from it using an ad hoc procedure. Abrahamsen et al. (1996) utilize a rejection sampling approach, but point out that this approach will not be feasible in practice due to immense processing requirements. In the current paper the seismic inverse problem is defined in a stochastic model defined by the graph in Figure 5, and a relatively efficient sampling algorithm for the posterior model is defined. Often, the seismic pulse or wavelet is estimated by a separate procedure and then assumed to be known in the seismic inversion. Here it is characterized by a wavelet parameter which is simultaneously estimated. The approach is demonstrated on data from the Troll petroleum reservoir in the North Sea. See also Hegstad & Omre (1998) for application to an even larger, three-dimensional data set.

2 The Troll Field data set

The Troll Field is the world's second largest offshore natural gas field and it also contains considerable amounts of oil. It is located in the Norwegian North Sea at a depth of approximately 1500 m below sea level. Reliable mapping and efficient depletion of this reservoir have great impact on the Norwegian economy, and on the stability of gas supply to the consumers in Europe.

The spatial variables to be modeled in this study are: porosity, acoustic impedance and seismic reflection coefficients. The focus is on representing the uncertainty about porosity over the reservoir domain $\mathcal{D}$. In this study the methodology is demonstrated on a representative two-dimensional cross section through the gas zone of the Troll reservoir, ie $\mathcal{D} \subset \mathbb{R}^2$, although the ultimate aim is to define the model in three dimensions. This is kept in mind when making the model assumptions.

The location of the cross section being studied is displayed in Figure 1. The reservoir variables of interest are $\{\Phi(x,t), Z(x,t), C(x,t); x \in \mathcal{D}^o, t \in \mathcal{T}^o\}$ being porosity, impedance and reflection coefficients, respectively. The domain $\mathcal{D}^o$ coincides with the seismic line and $\mathcal{T}^o$ is a window of seismic travel times representing depth. Depth representation by seismic travel time is a standard practice in the geophysical community, although a depth conversion must be done at a later stage. This conversion is not further discussed here. There are two types of reservoir specific observations available: seismic amplitude data and well observations.

The seismic amplitude data, see Figure 2, are post-stack, that is, preprocessed in order to improve the signal to noise ratio, see Dobrin & Savit (1988). The data are available on a grid with unit (20 m $\times$ 2 ms) covering $\mathcal{D}^o \times \mathcal{T}^o$, denoted $\mathcal{L}_{\mathcal{D}^o} \times \mathcal{L}_{\mathcal{T}^o}$. According to the frequently used seismic convolution model, see Dobrin & Savit (1988), the seismic amplitude data at $(x,t) \in \mathcal{L}_{\mathcal{D}^o} \times \mathcal{L}_{\mathcal{T}^o}$ are related to the reflection coefficients by:

$$S^o(x,t) = \int_{\mathcal{T}} w(t;\psi) C(x, t-s)\, ds + U_{S^o}(x,t), \tag{1}$$

with $w(t;\psi) = (1 - 2\pi^2\psi^2 t^2)e^{-\pi^2\psi^2 t^2}$ being a Ricker wavelet with parameter ψ; and $U_{S^o}(\cdot\,,\cdot)$ being a white noise observation error with variance $\sigma^2_{S^o}$.

The well observations, see Figure 3, are not located exactly in the cross section being studied, see Figure 1. This is ignored here, and the wells are assigned the location of seismic trace 47 and 142 respectively. The observations consist of porosity and impedance measurements at every ms down the vertical wells, defining $\mathcal{L}^w_{\mathcal{T}^o}$ The spatial averaging of these measurements is small compared to the scale being studied, hence the well observations at $(x,t) \in [x_{47}, x_{142}] \times \mathcal{L}^w_{\mathcal{T}^o}$, are,

$$\begin{aligned} \Phi^o(x,t) &= \Phi(x,t) + U_{\Phi^o}(x,t) \\ Z^o(x,t) &= Z(x,t) + U_{Z^o}(x,t) \end{aligned} \tag{2}$$

with $U_{\Phi^o}(\cdot\,,\cdot)$ and $U_{Z^o}(\cdot\,,\cdot)$ being white noise observation error terms with variance $\sigma^2_{\Phi^o}$ and $\sigma^2_{Z^o}$ respectively. Note in particular that the well observations are made at twice the vertical density of the seismic data. In Figure 3, a set of seismic reflection coefficients are also displayed, but these have been computed from the impedance observations, as explained later.

The reservoir specific observations actually available are represented by the high-dimensional vector $(\boldsymbol{\phi}^o, \boldsymbol{z}^o, \boldsymbol{s}^o)$, displayed in Figure 2 and 3.

3 Stochastic model

The study is actually performed on the part of the Troll cross section outlined in Figure 2. The vertical coordinate system is defined relative to the top horizon, and the area is denoted $\mathcal{D} \times \mathcal{T}$. The reservoir variables of interest are discretized into a (170×50) grid of unit size (20 m $\times$ 1 ms) over this area, defining $\mathcal{L}_\mathcal{D} \times \mathcal{L}_\mathcal{T}$. This grid coincides with the seismic traces horizontally and has the density of the well observations vertically, see Figure 4. This defines the vector of reservoir variables of interest:

$$(\boldsymbol{\Phi}, \boldsymbol{Z}, \boldsymbol{C}) : \{\Phi(x,t), Z(x,t), C(x,t) \quad ; \quad (x,t) \in \mathcal{L}_\mathcal{D} \times \mathcal{L}_\mathcal{T}\}. \tag{3}$$

Note further that whenever the reservoir specific observations $(\boldsymbol{\phi}^o, \boldsymbol{z}^o, \boldsymbol{s}^o)$ are referred to hereafter, they are represented in the system defined by $\mathcal{L}_\mathcal{D} \times \mathcal{L}_\mathcal{T}$.

The objective is to characterize the conditional pdf of the reservoir variables given the well observations and seismic data, ie $f(\boldsymbol{\phi}, \boldsymbol{z}, \boldsymbol{c} | \boldsymbol{\phi}^o, \boldsymbol{z}^o, \boldsymbol{s}^o)$, which can be written

$$f(\boldsymbol{\phi}, \boldsymbol{z}, \boldsymbol{c} | \boldsymbol{\phi}^o, \boldsymbol{z}^o, \boldsymbol{s}^o) = \text{const} \cdot f(\boldsymbol{\phi}^o, \boldsymbol{z}^o, \boldsymbol{s}^o | \boldsymbol{\phi}, \boldsymbol{z}, \boldsymbol{c}) \cdot f(\boldsymbol{\phi}, \boldsymbol{z}, \boldsymbol{c})$$

with the second term on the right hand side being the observation likelihood model and the third term being the prior model.

This conditional pdf will only under very strict assumptions about linearity and Gaussianity be subject to complete analytical evaluation. On the other hand, one may sample from it using a general Markov chain Monte Carlo algorithm. This is in most cases extremely resource requiring due to the high dimensionality and complicated conditioning, and is in practice prohibited. It will be even more so, when full three-dimensional models are considered. Here the problem is addressed by careful modeling of the physical relations involved and by making one simplifying assumption on the error structure of the likelihood, in order to obtain a highly efficient sequential sampling procedure. The graph in Figure 5 summarizes the stochastic model, and will be explained in the following sections.

4 Prior model

The prior stochastic model is denoted $f(\boldsymbol{\phi}, \boldsymbol{z}, \boldsymbol{c})$. In geophysics it is usually assumed, see for example Rasmussen & Maver (1996), that porosity and acoustic impedance are negatively correlated. This is incorporated in the following prior model for porosity at $(x,t) \in \mathcal{L}_{\mathcal{D}} \times \mathcal{L}_{\mathcal{T}}$:

$$[\Phi(x,t)|\boldsymbol{z}] = \mu_\Phi(z(x,t)) + U_\Phi(x,t) \tag{4}$$

with $\mu_\Phi(\cdot)$ being a function of the impedance in location (x,t) only; and $U_\Phi(\cdot,\cdot)$ being a discretized Gaussian random field with expectation zero and covariance matrix Σ_Φ defined by the spatial covariance function $\sigma^2_\Phi \rho_\Phi(\cdot)$. Figure 6 contains various displays of the well porosity and impedance observations. From the scatter plot in Figure 6a it can be justified that $\mu_\Phi(z) = 0.543 - 4.53 \cdot 10^{-5} \cdot z$. The residual plot in Figure 6b, assuming $\sigma^2_{\Phi^o}$ being relatively small, justifies $U_\Phi(\cdot,\cdot)$ being Gaussian with variance $\sigma^2_\Phi = 0.0331^2$. The spatial correlation function can be estimated in the vertical direction, see Figure 6c, but not horizontally. The correlation function is assumed to be of exponential form:

$$\rho(\Delta x, \Delta t; a_x, a_t, \nu) = \exp\{-3[(\frac{\Delta x}{a_x})^2 + (\frac{\Delta t}{a_t})^2]^{\nu/2}\}$$

with parameters $a_x = 540$, $a_t = 4.0$ and $\nu = 1.2$. The choices for a_t and ν are justified by Figure 6c. The value of a_x is chosen somewhat less than the corresponding value for the reflection coefficients, which later will be inferred from seismic data. This completes the definition of $f(\boldsymbol{\phi}|\boldsymbol{z})$ represented by a single arrow from $\boldsymbol{Z}$ to $\boldsymbol{\Phi}$ in Figure 5.

From geophysical theory, see Sheriff & Geldart (1982), it is known that reflection coefficients and acoustic impedance are non-linearly related. The expression on the grid $\mathcal{L}_{\mathcal{D}} \times \mathcal{L}_{\mathcal{T}}$ is:

$$\begin{aligned} C(x_i,t_j) &= \frac{Z(x_i,t_{j+1}) - Z(x_i,t_j)}{Z(x_i,t_{j+1}) + Z(x_i,t_j)}, \\ Z(x_i,t_{j+1}) &= \frac{1 + C(x_i,t_j)}{1 - C(x_i,t_j)} \cdot Z(x_i,t_j). \end{aligned} \tag{5}$$

Hence, given the impedance on the top horizon, $\boldsymbol{z}_{\text{top}} : \{z(x,t_0); x \in \mathcal{L}_{\mathcal{D}}\}$, there is a one-to-one non-linear relation between reflection coefficients $\boldsymbol{C}$ and impedances $\boldsymbol{Z}$. Assuming that the well observation of impedances are exact, ie $\sigma^2_{Z^o} = 0$, one can compute the exact reflection coefficients along the wells, see Figure 3. Denote these $\boldsymbol{c}^o$. The impedance $\boldsymbol{Z}$ can be computed by the non-linear deterministic relation above, given $\boldsymbol{c}$ and $\boldsymbol{z}_{\text{top}}$. This is represented by double arrows in Figure 5. The impedance of the top horizon is chosen such that vertically averages interpolate the wells observations of acoustic impedance linearly. A more formalized approach may be used, and that could be subject to further research. This defines $f(\boldsymbol{z}|\boldsymbol{c})$ as a Dirac pdf, suppressing the dependence on $\boldsymbol{z}_{\text{top}}$ in the notation.

The estimated reflection coefficients along the wells, see Figure 3, are used to justify the prior stochastic model for the reflection coefficients, $\boldsymbol{C}$. These are assumed to be a discretized Gaussian random field with expectation zero and covariance matrix Σ_C defined by the spatial covariance function $\sigma_C^2 \rho_C(\cdot)$. From Figure 7a it can be seen that the histogram appears as somewhat more heavy-tailed than Gaussian. Hence assuming a t-distributed random field, see Røislien (1998), may have been more appropriate. In spite of this a Gaussian assumption is used in order to have a familiar model. Note further that the reflection coefficients take values on $[-1, 1]$. The fact that none of the observations exceed 0.25 in absolute value means that this truncation is of no practical importance. The variance is set to $\sigma_C^2 = 0.035^2$, justified by Figure 7a. The correlation function is defined to be:

$$\rho_C(\Delta x, \Delta t; a_x, a_t, \nu) = [2(1 - \rho(0, 1; a_x, a_t, \nu))]^{-1} \cdot \\ [2\rho(\Delta x, \Delta t; a_x, a_t, \nu) - \rho(\Delta x, \Delta t + 1; a_x, a_t, \nu) - \rho(\Delta x, \Delta t - 1; a_x, a_t, \nu)]$$

with $\rho(\cdot)$ being the exponential correlation function previously defined. This relatively complex expression appears from linearizing Expression (5) and assuming acoustic impedance to be a relatively smoothly varying spatial variable. Note that this correlation function entails vertical pseudo-periodicity in the reflection coefficients since it takes negative values for certain Δt. This effect is recognized in the geophysical community, see Todoenschuck & Jensen (1988). The choice of parameters $a_t = 15$ and $\nu = 1.2$ is justified by Figure 7b. The horizontal range a_x can be inferred from the seismic observations by observing that at $\{(x', t'), (x'', t'')\} \in \mathcal{L}_{\mathcal{D}^o} \times \mathcal{L}_{\mathcal{T}^o}$:

$$\begin{aligned} &\mathrm{Cov}\{S^o(x', t'), S^o, (x'', t'')\} \\ &\qquad = \int_{\mathcal{T}} \int_{\mathcal{T}} w(t'; \psi) w(t''; \psi) \mathrm{Cov}\{C(x', t' - s), C(x'', t'' - u)\}\, ds\, du \\ &\qquad\qquad + \sigma_{S^o}^2 \delta(x' - x'', t' - t'')) \end{aligned}$$

with $\delta(\cdot\,, \cdot)$ being the Dirac delta function. Hence the extent of the horizontal dependence of the reflection coefficients is closely related to the horizontal dependence of the seismic data. By using this fact, the parameter is set to $a_x = 800$. This completes the definition of the prior model for the reflection coefficients, $f(\boldsymbol{c})$.

Hence the prior stochastic model for the reservoir variables of interest $(\boldsymbol{\Phi}, \boldsymbol{Z}, \boldsymbol{C})$ is defined through $f(\boldsymbol{\phi}, \boldsymbol{z}, \boldsymbol{c}) = f(\boldsymbol{\phi}|\boldsymbol{z})f(\boldsymbol{z}|\boldsymbol{c})f(\boldsymbol{c})$. In Figure 8 four realizations of porosity and acoustic impedance, $(\boldsymbol{\Phi}, \boldsymbol{Z})$, based on this prior pdf, are displayed. These realizations will of course not be conditioned to the available observations $(\boldsymbol{\phi}^o, \boldsymbol{z}^o, \boldsymbol{s}^o)$, but they do expose the consequences on structure and variability enforced by the prior model.

5 Likelihood model

The likelihood model for the observations, $f(\boldsymbol{\phi}^o, \boldsymbol{z}^o, \boldsymbol{s}^o | \boldsymbol{\phi}, \boldsymbol{z}, \boldsymbol{c})$ must be based on the geophysical relations defined in Section 2 and the discretization of the reservoir variables of interest.

The seismic amplitude data is defined by Expression (1), and can be written:

$$[\boldsymbol{S}^o | \boldsymbol{c}, \psi] = A_s(\psi) \cdot \boldsymbol{c} + \boldsymbol{U}_{S^o} \tag{6}$$

with $A_S(\psi)$ being a matrix defined by the seismic wavelet parameterized by ψ; and $\boldsymbol{U}_{S^o}$ being the vector of independent, centered Gaussian error terms with variance $\sigma^2_{S^o} = 0.182^2$. Assessment of the latter is based on seismic experience of observation and processing error. This defines $f(\boldsymbol{s}^o | \boldsymbol{c}, \psi)$, represented by single arrows from $\boldsymbol{C}$ and ψ to $\boldsymbol{S}^o$ in Figure 5. The value of the wavelet parameter is also highly uncertain, and based on seismic experience it is assigned a Gaussian prior pdf, $f(\psi)$, with expectation 40 and variance 20^2.

The well observations are defined by Expression (2), and can be written:

$$\begin{aligned} [\boldsymbol{\Phi}^o | \boldsymbol{\phi}] &= A_w \cdot \boldsymbol{\phi} + \boldsymbol{U}_{\Phi^o} \\ [\boldsymbol{Z}^o | \boldsymbol{z}] &= A_w \cdot \boldsymbol{z} \end{aligned} \tag{7}$$

with A_w being a matrix defined by the well locations; and $\boldsymbol{U}_{\Phi}$ being the vector of independent centered Gaussian error terms with covariance matrix Σ_{Φ^o} In this particular case study the variance is set to zero. Note that the impedances along the well trace must be exact observations, hence no error term. This entails that from Expression (5) one obtains:

$$[\boldsymbol{C}^o|\boldsymbol{c}] = A_w \cdot \boldsymbol{c}. \tag{8}$$

Moreover, this exactness assumption is required in order to simplify the sampling algorithm as will be shown in the next section. This defines the likelihood models, $f(\boldsymbol{\phi}^o|\boldsymbol{\phi})$, $f(\boldsymbol{z}^o|\boldsymbol{z})$ and $f(\boldsymbol{c}^o|\boldsymbol{c})$, which are represented by single or double arrows on Figure 5, dependent on whether exact observations are required or not. Adding assumptions about independence of the error terms in the likelihood models for the various data acquisition procedures, this entails that:

$$f(\boldsymbol{\phi}^o, \boldsymbol{z}^o, \boldsymbol{s}^o|\boldsymbol{\phi}, \boldsymbol{z}, \boldsymbol{c}) = \int f(\boldsymbol{s}^o|\boldsymbol{c}, \psi) \cdot f(\boldsymbol{\phi}^o|\boldsymbol{\phi}) \cdot f(\boldsymbol{z}^o|\boldsymbol{z}) \cdot f(\psi)\, d\psi$$

6 Posterior model

The two reservoir variables of primary interest are porosity and acoustic impedance, hence the posterior $f(\boldsymbol{\phi}, \boldsymbol{z}|\boldsymbol{\phi}^o, \boldsymbol{z}^o, \boldsymbol{c}^o, \boldsymbol{s}^o)$. Recall that $\boldsymbol{z}^o$ and $\boldsymbol{c}^o$ contain identical information due to Expression (5). However, the model also contains two other unknowns, the reflection coefficients, $\boldsymbol{C}$, and the wavelet parameter, ψ, see Figure 5. Hence it is more convenient to evaluate the pdf $f(\boldsymbol{\phi}, \boldsymbol{z}, \boldsymbol{c}, \psi|\boldsymbol{\phi}^o, \boldsymbol{z}^o, \boldsymbol{c}^o, \boldsymbol{s}^o)$. By sampling from this pdf and only retaining the $(\boldsymbol{\phi}, \boldsymbol{z})$-entries, one obtains samples of the variables of primary interest.

Consider the obvious factorization:

$$\begin{aligned} f(\boldsymbol{\phi}, \boldsymbol{z}, \boldsymbol{c}, \psi|\boldsymbol{\phi}^o, \boldsymbol{z}^o, \boldsymbol{c}^o, \boldsymbol{s}^o) =& f(\boldsymbol{\phi}|\boldsymbol{z}, \boldsymbol{c}, \psi, \boldsymbol{\phi}^o, \boldsymbol{z}^o, \boldsymbol{c}^o, \boldsymbol{s}^o) \\ & \cdot f(\boldsymbol{z}|\boldsymbol{c}, \psi, \boldsymbol{\phi}^o, \boldsymbol{z}^o, \boldsymbol{c}^o, \boldsymbol{s}^o) \\ & \cdot f(\boldsymbol{c}|\psi, \boldsymbol{\phi}^o, \boldsymbol{z}^o, \boldsymbol{c}^o, \boldsymbol{s}^o) \\ & \cdot f(\psi|\boldsymbol{\phi}^o, \boldsymbol{z}^o, \boldsymbol{c}^o, \boldsymbol{s}^o) \end{aligned} \tag{9}$$

The first term on the right hand side, $f(\boldsymbol{\phi}|\boldsymbol{z}, \boldsymbol{c}, \psi, \boldsymbol{\phi}^o, \boldsymbol{z}^o, \boldsymbol{c}^o, \boldsymbol{s}^o)$, can from Figure 5 be seen to equal $f(\boldsymbol{\phi}|\boldsymbol{z}, \boldsymbol{\phi}^o)$.

The second term on the right hand side, $f(\boldsymbol{z}|\boldsymbol{c}, \psi, \boldsymbol{\phi}^o, \boldsymbol{z}^o, \boldsymbol{c}^o, \boldsymbol{s}^o)$, can from Figure 5 be seen to equal $f(\boldsymbol{z}|\boldsymbol{c})$. Recall that the dependence on $\boldsymbol{z}_{\text{top}}$ is suppressed in the notation.

The third term on the right hand side, $f(\boldsymbol{c}|\psi, \boldsymbol{\phi}^o, \boldsymbol{z}^o, \boldsymbol{c}^o, \boldsymbol{s}^o)$, is somewhat more complicated. Recall that due to Expression (5) and the assumption of no observations error, $\boldsymbol{z}^o$ and $\boldsymbol{c}^o$ are identical pieces of information with regard to $\boldsymbol{C}$. The conditioning on $\boldsymbol{\phi}^o$ complicates the expression, however, since $\boldsymbol{C}$ is non-linearly related to $\boldsymbol{\Phi}$ through $\boldsymbol{Z}$, see Expression (4) and (5). It can be shown under the current model assumptions, however, that:

$$f(\boldsymbol{c}|\psi, \boldsymbol{\phi}^o, \boldsymbol{z}^o, \boldsymbol{c}^o, \boldsymbol{s}^o) = f(\boldsymbol{c}|\psi, \boldsymbol{c}^o, \boldsymbol{s}^o). \tag{10}$$

The demonstration is as follows:

$$f(\boldsymbol{c}|\psi, \boldsymbol{\phi}^o, \boldsymbol{z}^o, \boldsymbol{c}^o, \boldsymbol{s}^o) = \frac{f(\boldsymbol{s}^o|\boldsymbol{c}, \psi) f(\psi|\boldsymbol{c}) f(\boldsymbol{\phi}^o|\boldsymbol{c}, \boldsymbol{z}^o) f(\boldsymbol{c}, \boldsymbol{z}^o)}{\int f(\boldsymbol{s}^o|\boldsymbol{\zeta}, \psi) f(\psi|\boldsymbol{\zeta}) f(\boldsymbol{\phi}^o|\boldsymbol{\zeta}, \boldsymbol{z}^o) f(\boldsymbol{\zeta}, \boldsymbol{z}^o)\, d\boldsymbol{\zeta}}$$

but since $\boldsymbol{z}^o$ and $\boldsymbol{\phi}^o$ are both observed everywhere along the wells, and since there is no observation error in $\boldsymbol{z}^o$ and the dependence in Expression (4) through $\mu_\Phi(\cdot)$ is only locationwise, one has $f(\boldsymbol{\phi}^o|\boldsymbol{c}, \boldsymbol{z}^o) = f(\boldsymbol{\phi}^o|\boldsymbol{z}^o)$. This entails that the corresponding term cancels in the fraction above, and hence the corresponding pdf does not depend on $\boldsymbol{\phi}^o$. Consequently, Expression (10) holds.

Finally, the fourth term on the right hand side, $f(\psi|\boldsymbol{\phi}^o, \boldsymbol{z}^o, \boldsymbol{c}^o, \boldsymbol{s}^o)$, is equal to $f(\psi|\boldsymbol{c}^o, \boldsymbol{s}^o)$ using similar arguments as above.

Consequently, the posterior pdf of interest can be factorized as:

$$f(\boldsymbol{\phi}, \boldsymbol{z}, \boldsymbol{c}, \psi|\boldsymbol{\phi}^o, \boldsymbol{z}^o, \boldsymbol{c}^o, \boldsymbol{s}^o) = f(\boldsymbol{\phi}|\boldsymbol{z}, \boldsymbol{\phi}^o) \cdot f(\boldsymbol{z}|\boldsymbol{c}) \cdot f(\boldsymbol{c}|\psi, \boldsymbol{c}^o, \boldsymbol{s}^o) \cdot f(\psi|\boldsymbol{c}^o, \boldsymbol{s}^o) \tag{11}$$

This entails that samples from the posterior pdf can be obtained by a sequential sampling procedure.

The first term on the right hand side of Expression (11) is defined by Expression (4) and (7). Because $\boldsymbol{\Phi}$ given $\boldsymbol{z}$ is Gaussian and the observations $\boldsymbol{\Phi}^o$ are linearly related to $\boldsymbol{\Phi}$ with a Gaussian error term, this conditional distribution is Gaussian with

$$\begin{aligned}
\mathrm{E}[\boldsymbol{\Phi}|\boldsymbol{z}, \boldsymbol{\phi}^o] &= \mu_\Phi(\boldsymbol{z}) + \Sigma_\Phi A_w^T (A_w \Sigma_\Phi A_w^T + \Sigma_{\Phi^o})^{-1} (\boldsymbol{\phi}^o - A_w \mu_\Phi(\boldsymbol{z})), \\
\mathrm{Cov}[\boldsymbol{\Phi}|\boldsymbol{z}, \boldsymbol{\phi}^o] &= \Sigma_\Phi - \Sigma_\Phi A_w^T (A_w \Sigma_\Phi A_w^T + \Sigma_{\Phi^o})^{-1} A_w \Sigma_\Phi.
\end{aligned}$$

The second term is a Dirac pdf, hence a deterministic relation, see Expression (5) with $\boldsymbol{z}_{\text{top}}$ implicitly given.

The third term of Expression (11) is obtained by a combination of the forward models of $\boldsymbol{C}^o$ and $\boldsymbol{S}^o$ from Expression (6) and (8). It gives

$$\left\{ \begin{bmatrix} \boldsymbol{C}^o \\ \boldsymbol{S}^o \end{bmatrix} \mid \boldsymbol{c}, \psi \right\} = \begin{bmatrix} A_w \\ A_s(\psi) \end{bmatrix} \boldsymbol{c} + \begin{bmatrix} 0 \\ \boldsymbol{U}_s \end{bmatrix},$$

in short

$$[(\boldsymbol{C}^o, \boldsymbol{S}^o)^T | \boldsymbol{c}, \psi] = A(\psi) \cdot \boldsymbol{c} + \boldsymbol{U}_D, \tag{12}$$

where $A(\psi)$ and $\boldsymbol{U}_D$ are defined by the expressions above. The error term $\boldsymbol{U}_D$ is Gaussian with zero mean and covariance matrix Σ_D. Because $\boldsymbol{C}$ has a Gaussian prior distribution and $\boldsymbol{C}^o$ and $\boldsymbol{S}^o$ are linear according to Expression (12), the distribution of $\boldsymbol{C}$, $\boldsymbol{C}^o$ and $\boldsymbol{S}^o$ given Ψ is multivariate Gaussian. It follows that the conditional pdf of $\boldsymbol{C}$ is Gaussian with:

$$\begin{aligned} \mathrm{E}[\boldsymbol{C}|\psi, \boldsymbol{c}^o, \boldsymbol{s}^o] &= \Sigma_C A^T(\psi)[A(\psi)\Sigma_C A^T(\psi) + \Sigma_D]^{-1}(\boldsymbol{c}^o, \boldsymbol{s}^o)^T, \\ \mathrm{Cov}[\boldsymbol{C}|\psi, \boldsymbol{c}^o, \boldsymbol{s}^o] &= \Sigma_C - \Sigma_C A^T(\psi)[A(\psi)\Sigma_C A^T(\psi) + \Sigma_D]^{-1} A(\psi)\Sigma_C. \end{aligned} \tag{13}$$

The fourth term of Expression (11) can be written

$$\begin{aligned} f(\psi|\boldsymbol{c}^o, \boldsymbol{s}^o) &= \text{const} \cdot f(\boldsymbol{s}^o|\psi, \boldsymbol{c}^o) \cdot f(\psi|\boldsymbol{c}^o) \\ &= \text{const} \cdot |\Sigma_{S^o|\psi,c^o}|^{-1/2} \cdot \exp\{-\frac{1}{2}(\boldsymbol{s}^o - \boldsymbol{\mu}_{S^o|\psi,c^o})^T \Sigma_{S^o|\psi,c^o}^{-1}(\boldsymbol{s}^o - \boldsymbol{\mu}_{S^o|\psi,c^o})\} \\ &\quad \cdot f(\psi), \end{aligned} \tag{14}$$

where

$$\begin{aligned} \boldsymbol{\mu}_{S^o|\psi,c^o} = \mathrm{E}[\boldsymbol{S}^o|\psi, \boldsymbol{c}^o] &= A_s(\psi)\mathrm{E}[\boldsymbol{C}|\boldsymbol{c}^o], \\ \Sigma_{S^o|\psi,c^o} = \mathrm{Cov}[\boldsymbol{S}^o|\psi, \boldsymbol{c}^o] &= A_s(\psi)\mathrm{Cov}[\boldsymbol{C}|\boldsymbol{c}^o]A_s^T(\psi) + \Sigma_S, \end{aligned}$$

and $f(\psi)$ is the prior pdf of the wavelet parameter Ψ. Here the conditional mean and variance of C given well observations are given by

$$\begin{aligned} \mathrm{E}[\boldsymbol{C}|\boldsymbol{c}^o] &= \Sigma_C A_w^T(A_w \Sigma_C A_w^T)^{-1}\boldsymbol{c}^o, \\ \mathrm{Cov}[\boldsymbol{C}|\boldsymbol{c}^o] &= \Sigma_C A_w^T(A_w \Sigma_C A_w^T)^{-1} A_w \Sigma_C. \end{aligned}$$

To summarize, sampling from the posterior pdf given in Equation (11) can be done by sequential sampling from a univariate pdf, $f(\psi|\boldsymbol{c}^o, \boldsymbol{s}^o)$, then from a multivariate Gaussian pdf, $f(\boldsymbol{c}|\psi, \boldsymbol{c}^o, \boldsymbol{s}^o)$; then a non-linear transformation defined by $f(\boldsymbol{z}|\boldsymbol{c})$; and lastly sampling from a multivariate Gaussian pdf, $f(\boldsymbol{\phi}|\boldsymbol{z}, \boldsymbol{\phi}^o)$.

7 Sampling Algorithms

The pdf $f(\psi|\boldsymbol{c}^o, \boldsymbol{s}^o)$, see Expression (14), is given as an unknown constant times a term that is high-dimensional and resource demanding to compute. Markov chain Monte Carlo (McMC) methods, which are otherwise often used when the normalization constant is unknown, would be an inefficient use of the resource-demanding computations for this low-dimensional pdf. The approach chosen here is to approximate the pdf $f(\psi|\boldsymbol{c}^o, \boldsymbol{s}^o)$ by a sum of orthogonal polynomials and to sample from this by rejection sampling. To be more specific, it is $\ln\{f(\psi|\boldsymbol{c}^o, \boldsymbol{s}^o)\}$ that is approximated up to an additive constant, since this ensures non-negativity in the approximation and is sufficient for later sampling.

The approximation is based on normalized Hermite polynomials, $H_i(x)/\sqrt{i!}\ ;\ i = 0, 1, \ldots$ with $H_0(x) = 1$, $H_1(x) = x$ and $H_{i+1}(x) = xH_i(x) - nH_{i-1}(x)\ ;\ i = 2, 3, \ldots$. For a given order in the approximation, n, it is known that the interpolation at the roots of the polynomial $H_{n+1}(x)$ will minimize the integrated squared approximation error with respect to the weight function $\exp(-\frac{1}{2}x^2)$, see Johnson & Riess (1982) and Abramowitz & Stegun (1972).

A polynomial of order $n = 14$ is found to be suitable. The pdf $f(\psi|\boldsymbol{c}^o, \boldsymbol{s}^o)$ is computed up to a multiplicative constant in the 15 roots of the Hermite polynomial $H_{15}(\frac{\psi-\mu}{\sigma})$ with μ being the prior expectation of ψ, ie 40; and σ being set to 3. This defines the coefficients in the polynomial approximation. The resulting approximation is presented in Figure 9. In order to sample from $f(\psi|\boldsymbol{c}^o, \boldsymbol{s}^o)$, a rejection sampling algorithm, see Ripley (1987), is used to sample from this approximation to the pdf. The envelope is defined to be piecewise linear in the logarithmic transformation, see Figure 9.

The pdf $f(\boldsymbol{c}|\psi, \boldsymbol{c}^o, \boldsymbol{s}^o)$, see Expression (13), is multivariate Gaussian with dimension identical to the dimension of the grid representation $\mathcal{L}_\mathcal{D} \times \mathcal{L}_\mathcal{T}$. In three dimensional studies this may be in the range 10^6—10^9. The conditioning variable $\boldsymbol{s}^o$ is also of high dimension; in the present case the dimension of the vector $\boldsymbol{s}^o$ is half the dimension of $\boldsymbol{c}$. Moreover, several samples from $f(\boldsymbol{c}|\psi, \boldsymbol{c}^o, \boldsymbol{s}^o)$ are normally required. Hence it is of utmost importance to use an efficient sampling algorithm. A sequential algorithm along the lines of the ones presented in Ripley (1987) and Omre, Sølna & Tjelmeland (1993) is defined. Note further that during the generation of the first sample several findings are stored for use in the generation of the subsequent samples.

Define the decomposition $\boldsymbol{c} = (\boldsymbol{c}^o, \boldsymbol{c}') = (\boldsymbol{c}^o, c'_1, \dots, c'_m)$ with $\boldsymbol{c}'$ being the vector of unobserved elements in $\boldsymbol{c}$, and consider the factorization:

$$\begin{aligned} f(\boldsymbol{c}|\psi, \boldsymbol{c}^o, \boldsymbol{s}^o) &= f(c'_m|c'_{m-1}, \dots, c'_1, \boldsymbol{c}^o, \boldsymbol{s}^o, \psi) \\ &\quad \cdot f(c'_{m-1}|c'_{m-2}, \dots, c'_1, \boldsymbol{c}^o, \boldsymbol{s}^o, \psi) \cdot \ldots \cdot f(c'_2|c'_1, \boldsymbol{c}^o, \boldsymbol{s}^o, \psi) \cdot f(c'_1|\boldsymbol{c}^o, \boldsymbol{s}^o, \psi). \end{aligned}$$

All these factors are multivariate Gaussian and subject to full analytical evaluation. The only problem is the dimensionality of the conditioning, which eventually reaches the full dimensionality of the problem. The approximate algorithm being used replaces each factor with a pdf conditioned only on a subset of the actual conditioning variables. The spatial nature of the problem, and the fact that spatial closeness is linked to correlation, is used in the selection of the subset.

Consider the factor $f(c'_i|c'_{i-1}, \dots, c'_1, \boldsymbol{c}^o, \boldsymbol{s}^o, \psi) = f(c'_i|a_i, \psi)$ with $a_i = (c'_{i-1}, \dots, c'_1, \boldsymbol{c}^o, \boldsymbol{s}^o)$ and $\mathcal{A}_i$ its stochastic counterpart. Let $\mathcal{B}_i$ be a subset of $\mathcal{A}_i$ and $\mathcal{B}_i^*$ its complement. Let $\tilde{C}_i$ be the approximation obtained by replacing a sample from $f(c'_i|a_i, \psi)$ by a sample from $f(c'_i|b_i, \psi)$. Start with $\mathcal{B}_i = \emptyset$ and perform the following iterations: Move the element Y_k in $\mathcal{B}_i^*$ that maximizes $|\mathrm{corr}(C_i, Y_k) - \mathrm{corr}(\tilde{C}_i, Y_k)|$ into $\mathcal{B}_i$ if the absolute correlation exceeds the threshold δ. Iterate until no candidate in $\mathcal{B}_i^*$ can be found. In practice, not all elements in $\mathcal{B}_i^*$ have to be evaluated since some of them exclude themselves by being located far from C'_i. The factor $f(c'_i|a_i, \psi)$ is now replaced by $f(c'_i|b_i, \psi)$ with b_i, being the realization of $\mathcal{B}_i$. The fact that the correlations computed above will only be dependent on the spatial configuration of $\mathcal{A}_i$ and not on the actual realization, entails that corresponding approximations can be used also when obtaining subsequent samples. In the actual sampling used here, the value of δ is set to 0.001.

The approximate sampling procedure is evaluated on a small test case. Consider a Gaussian random field on a domain $[250 \times 250]$ with expectation zero, unit variance and an exponential correlation functions with parameters $\Delta x = \Delta t = 20$ and $\nu = 1$. Let the field be discretized on a grid of size $[250 \times 250]$ and the representation be denoted $\boldsymbol{Y}$. The conditioning set, $\mathcal{A}$, consists of three point observations in the upper left corner of Y and a $[250 \times 250]$ grid of weighted averages of vertical grid nodes, where the weights are calculated using a 40 Hz Ricker wavelet, with the vertical distance between grid nodes set to 1 ms and the length of the wavelet 37 grid nodes. The evaluation procedure is: Generate an unconditional sample $\boldsymbol{y}$ from $f(\boldsymbol{y})$. Let a be a realization of $\mathcal{A}$ from $\boldsymbol{y}$. Use the approximate sampling procedure to generate $\boldsymbol{y}_s$ from $f(\boldsymbol{y}|a)$. If an exact algorithm was used, $\boldsymbol{y}_s$ would be Gaussian according to $f(\boldsymbol{y})$. This procedure is repeated 1000 times, and the results are summarized in Figure 10. The first line in the figure displays one sample, the locationwise average and the locationwise empirical variance of the 1000 samples. No artifacts can be observed. Line two displays the locationwise empirical covariance, $\widehat{\text{Cov}}\{Y(x,t), Y(x+i, t+j)\}$ for $(i,j) = (1,1)$, $(3,4)$ and $(10,10)$ respectively; and the last line displays the corresponding histograms and the true values obtained by the spatial correlation function. Again excellent agreement between sampling results and model parameters is found. It is concluded that the approximate algorithm is reliable.

To summarize, a sample from $f(\boldsymbol{\phi}, \boldsymbol{z}, \boldsymbol{c}, \psi|\boldsymbol{\phi}^o, \boldsymbol{z}^o, \boldsymbol{c}^o, \boldsymbol{s}^o)$, see Expression (11), is obtained by a sequence of operations: First sample from $f(\psi|\boldsymbol{c}^o, \boldsymbol{s}^o)$ by the algorithm described previously; thereafter sample from $f(\boldsymbol{c}|\psi, \boldsymbol{c}^o, \boldsymbol{s}^o)$ by the algorithm also previously described; then transform into $\boldsymbol{z}$ by using $f(\boldsymbol{z}|\boldsymbol{c}, \boldsymbol{z}^o)$; and last sample from $f(\boldsymbol{\phi}|\boldsymbol{z}, \boldsymbol{\phi}^o)$.

8 Results

Samples from $f(\boldsymbol{\phi}, \boldsymbol{z}, \boldsymbol{c}, \psi|\boldsymbol{\phi}^o, \boldsymbol{z}^o, \boldsymbol{c}^o, \boldsymbol{s}^o)$ are generated by the simulation algorithm described in the previous section.

Based on 2000 posterior samples of the seismic wavelet parameter ψ, estimates of expectation and variance are 43.4 and 1.12^2 respectively. This should be compared to the corresponding parameters in the prior pdf $f(\psi)$ being 40 and 20^2 respectively, see Figure 9. Hence it is obvious that the well observations and seismic data carry substantial information about the seismic wavelet parameter ψ. This is important in order to utilize the seismic data efficiently.

In Figure 11, four pairs of posterior porosity and acoustic impedance samples are displayed. By comparing these to the samples from the prior pdf $f(\boldsymbol{\phi}, \boldsymbol{z})$, see Figure 8, one observes that the conditioning enforces certain patterns on the samples. These characteristics are crucial when, at a later stage, one needs to simulate fluid flow through the reservoir. In Figure 12, the locationwise average and empirical standard deviation over 10 samples from the posterior pdf of the porosity being estimates of $\mathrm{E}\{\boldsymbol{\Phi}|\boldsymbol{\phi}^o, \boldsymbol{z}^o, \boldsymbol{s}^o\}$ and $\mathrm{SD}\{\boldsymbol{\Phi}|\boldsymbol{\phi}^o, \boldsymbol{z}^o, \boldsymbol{s}^o\}$ respectively, are presented. Recall that the corresponding parameters in the prior pdf are constant over the domain. This improved spatial prediction of porosity can be used to locate infill wells more efficiently.

A closer look at Figure 11 reveals some artifacts around the well at location $x = 142$. This is possibly due to the well observations actually being located somewhat off the seismic line being studied.

In Figure 13, the simulated seismic amplitudes based on the four samples from the posterior pdf in Figure 11 are displayed. Note that these do not include seismic observation error. Comparing these to the actual seismic data in Figure 4, one observes an amazing agreement. The lower display contains the difference between the actual data set and the 10 posterior samples. If the seismic model had been correct one would expect this to display the observation error being white noise. There is still some spatial structure to be modeled, but most of it is captured by the model.

The current model conditions the posterior pdf of the wavelet parameter to all well observations and seismic data. In practice seven seismic traces in the vicinity of each well are used. Figure 14 shows that this reduces the uncertainty in the posterior pdf considerably compared to the one-trace-per-well approach traditionally used. This reduction in uncertainty is important since the seismic wavelet is used in the processing of seismic data in large areas without well control.

The contribution of seismic data can be observed by comparing Figure 15 and Figure 12. Both figures display averages and empirical standard deviation over 10 samples of porosity. The former figure represents conditioning on well observations only, while the latter represents conditioning to both well observations and seismic data. The seismic data are shown to carry crucial information about the spatial structure between the wells. Moreover, the prediction error is considerably reduced when including the seismic data. Acquisition of data is costly in reservoir evaluation, hence it is crucial to justify the importance by displays like this.

9 Conclusions

A statistical approach to seismic inversion clarifies the underlying assumptions and provides quantification of the uncertainty in the results. The ability to simultaneously estimate non-linear model parameters, like the wavelet parameter, and possibly others, is important since these are necessary to characterize the high-dimensional linear model. Quantifying the contribution of the various data sources to the overall reduction in uncertainty is important when efficient data acquisition strategies shall be defined. The established framework does also lend itself to inclusion of other data sources like well production tests, and to more sophisticated seismic models.

Acknowledgments

The work is partly funded by the Strategic University Program 'Uncertainty in Reservoir Evaluation', supported by the Research Council of Norway. The authors would like to thank the Troll License for permission to use data from the Troll Field, and Gyrid Johnsen and Åshild Skålnes at Norsk Hydro ASA for helpful comments and discussions on topics related to these data. We thank our colleagues Håkon Tjelmeland and Håvard Rue for helpful comments and suggestions. Fruitful discussions with persons in the SCRF-program during visits at the Department of Petroleum Engineering, Stanford University, have also been very beneficial.

References

Abrahamsen, P., Buland, A., Bølviken, E., Hauge, R., Hektoen, A. & Skorstad, A. (1996), Conditioning stochastic reservoir models on seismic amplitude traces — Stochastic inversion and simulation, NR-note SAND/07/1996, Norwegian Computing Center, P.O.Box 114 Blindern, N-0314 Oslo, Norway.

Abramowitz, M. & Stegun, I. A., eds (1972), *Handbook of Mathematical Functions*, 9th printing, Dover Publications, New York.

Bortoli, L.-J., Alabert, F., Haas, A. & Journel, A. (1993), Constraining stochastic images to seismic data: Stochastic simulation of synthetic seismograms, *in* A. Soares, ed., 'Geostatistics Tróia '92', Kluwer Academic Publishers, Dordrecht, pp. 325–337.

Dobrin, M. B. & Savit, C. H. (1988), *Introduction to Geophysical Prospecting*, 4th edn, McGraw-Hill Book Company.

Haas, A. & Dubrule, O. (1994), 'Geostatistical inversion - a sequential method of stochastic reservoir modeling constrained by seismic data', *First Break* **12**(11), 561–569.

Hegstad, B. K. & Omre, H. (1998), Reservoir characterization integrating well observations, seismic data and production history, Technical Report Statistics No. 11/98, Department of Mathematical Sciences, NTNU, N-7034 Trondheim, Norway.

Johnson, L. W. & Riess, R. D. (1982), *Numerical Analysis*, 2nd edn, Addison-Wesley, Reading, Massachusetts.

Omre, H. & Tjelmeland, H. (1997), Petroleum geostatistics, *in* E. Baafi & N. Schofield, eds, 'Geostatistics Wollongong '96', Kluwer Academic Publishers, Dordrecht, pp. 41–52.

Omre, H., Sølna, K. & Tjelmeland, H. (1993), Simulation of random functions on large lattices, *in* A. Soares, ed., 'Geostatistics Tróia '92', Kluwer Academic Publishers, Dordrecht, pp. 179–199.

Rasmussen, K. B. & Maver, K. G. (1996), Direct inversion for porosity of post stack seismic data, *in* 'European 3-D Reservoir modeling conference, Stavanger', Society of Petroleum Engineers, pp. 235–246. SPE 35509.

Ripley, B. D. (1987), *Stochastic Simulation*, John Wiley & Sons, New York.

Røislien, J. (1998), Random t-distributed fields, Technical Report Statistics No. 9/98, Department of Mathematical Sciences, NTNU, N-7034 Trondheim, Norway.

Sheriff, R. E. & Geldart, L. P. (1982), *Exploration Seismology. History, theory and data acquisition*, Cambridge University Press.

Tarantola, A. (1987), *Inverse Problem Theory*, Elsevier, Amsterdam.

Todoenschuck, J. P. & Jensen, O. G. (1988), 'Joseph geology and seismic deconvolution', *Geophysics* **53**(11), 1410–1414.

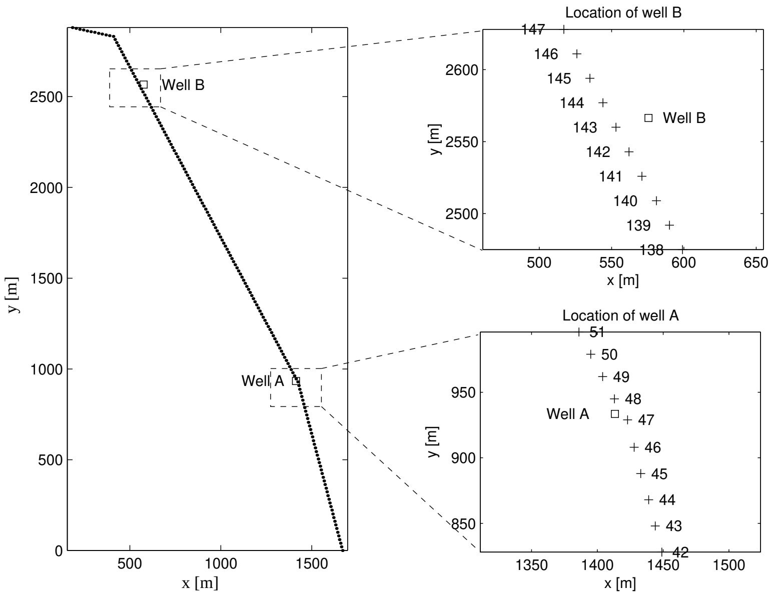

Figure 1: Location of the cross section to be studied, seismic line and well locations.

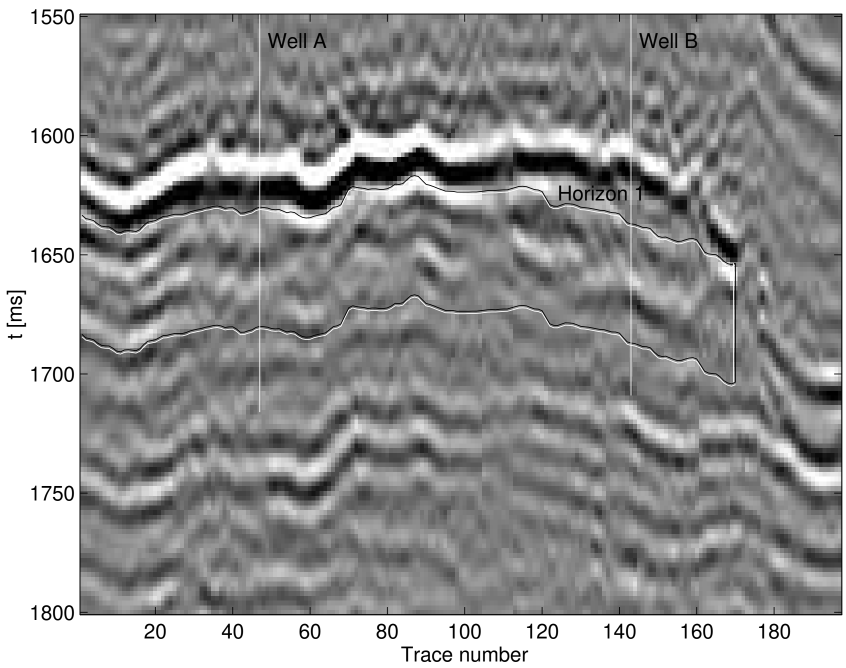

Figure 2: Section of seismic amplitude data ($\boldsymbol{s}^o$). Outline of study area.

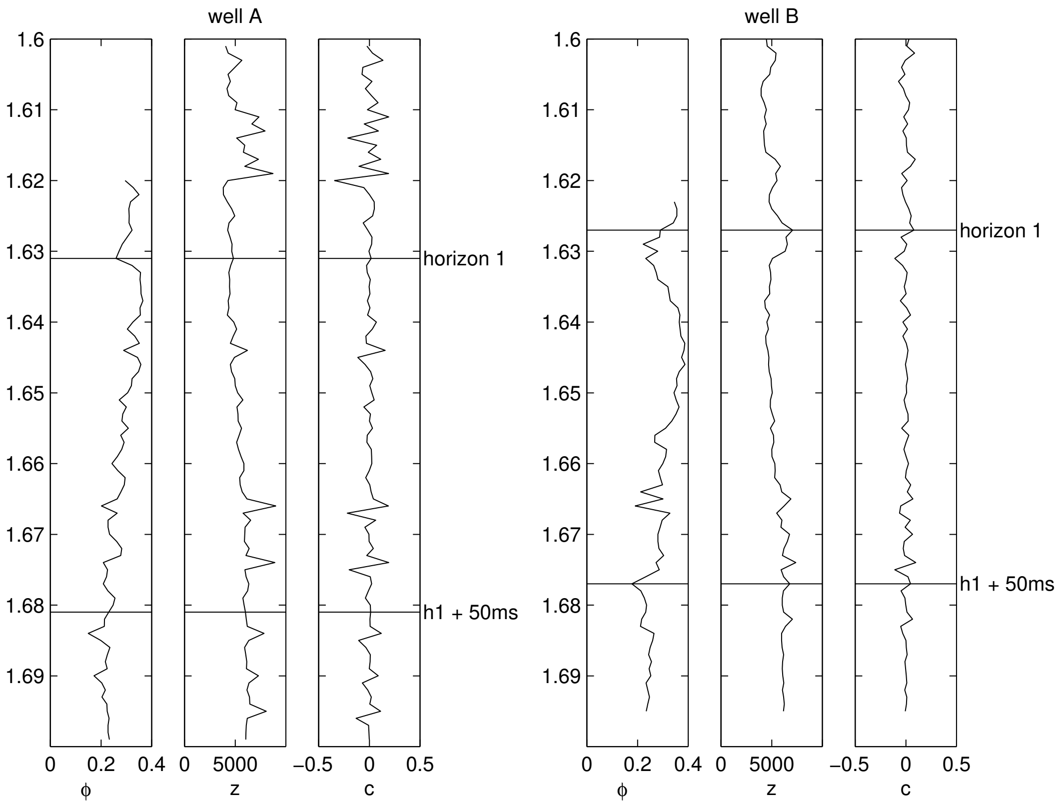

Figure 3: Well observations of porosity ($\boldsymbol{\phi}^o$), acoustic impedance ($\boldsymbol{z}^o$) and reflection coefficients ($\boldsymbol{c}^o$).

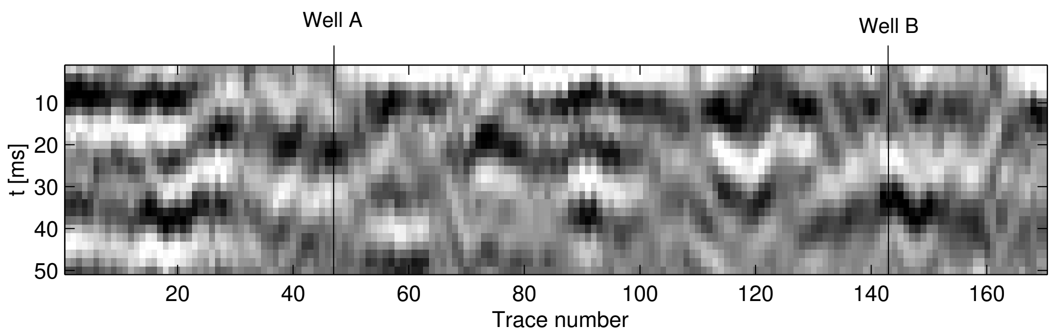

Figure 4: Cross section under study with well locations and seismic amplitude data.

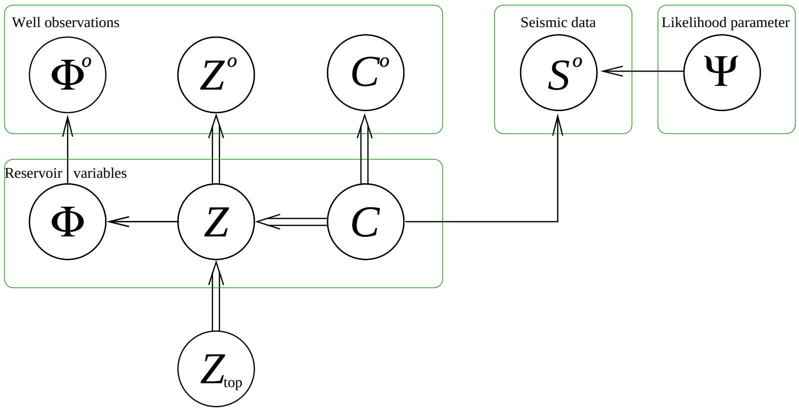

Figure 5: Graph of stochastic model.

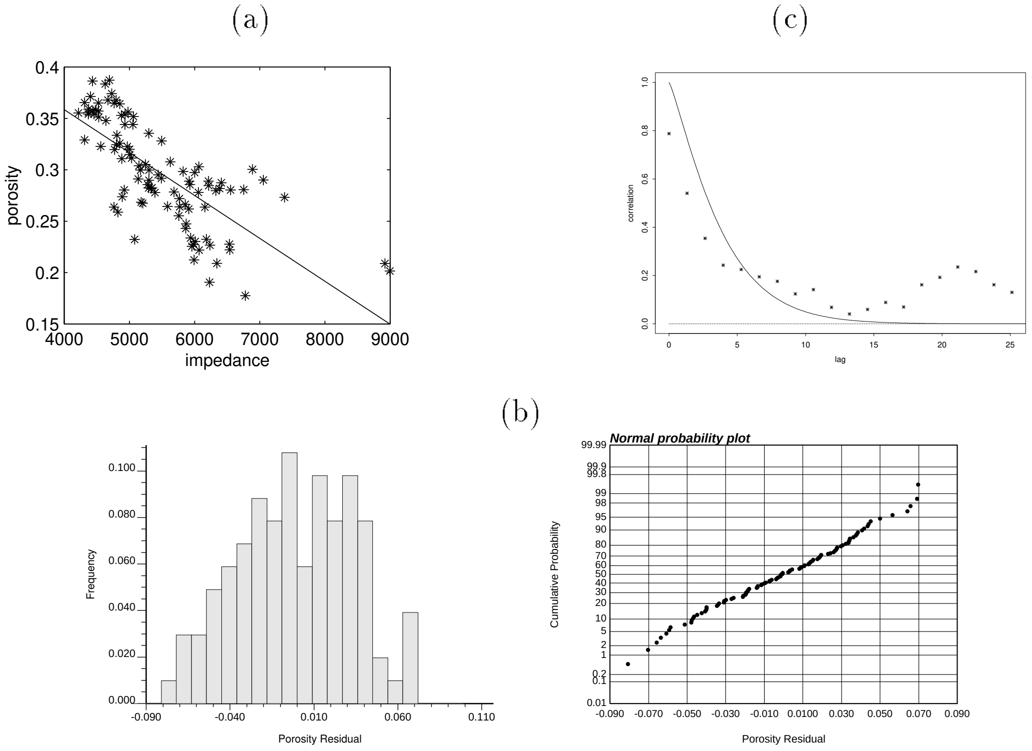

Figure 6: Well observations. (a) Scatter plot of porosity vs acoustic impedance with regression line. (b) Histogram and normal probability plot of porosity residuals. (c) Empirical correlation function of porosity residuals with model.

(a)

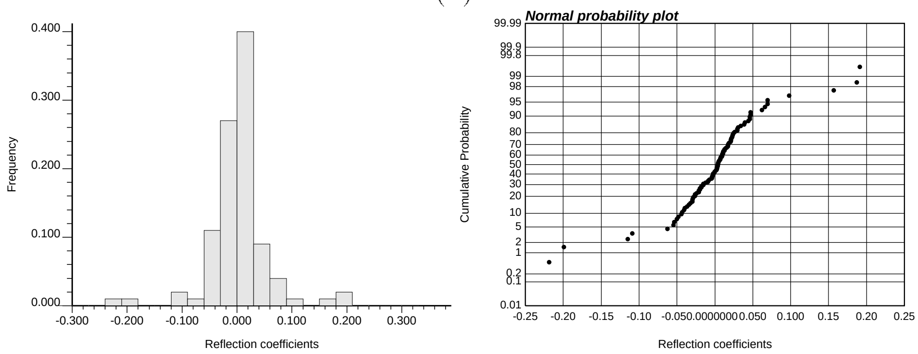

(b)

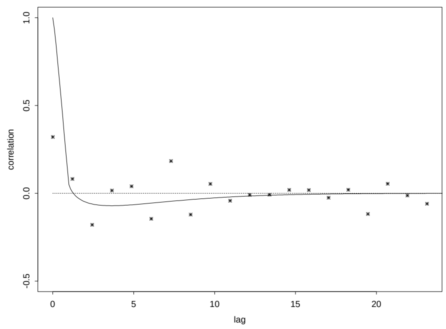

Figure 7: Well observations. (a) Histogram and normal probability plot of reflection coefficients. (b) Empirical correlation function with model

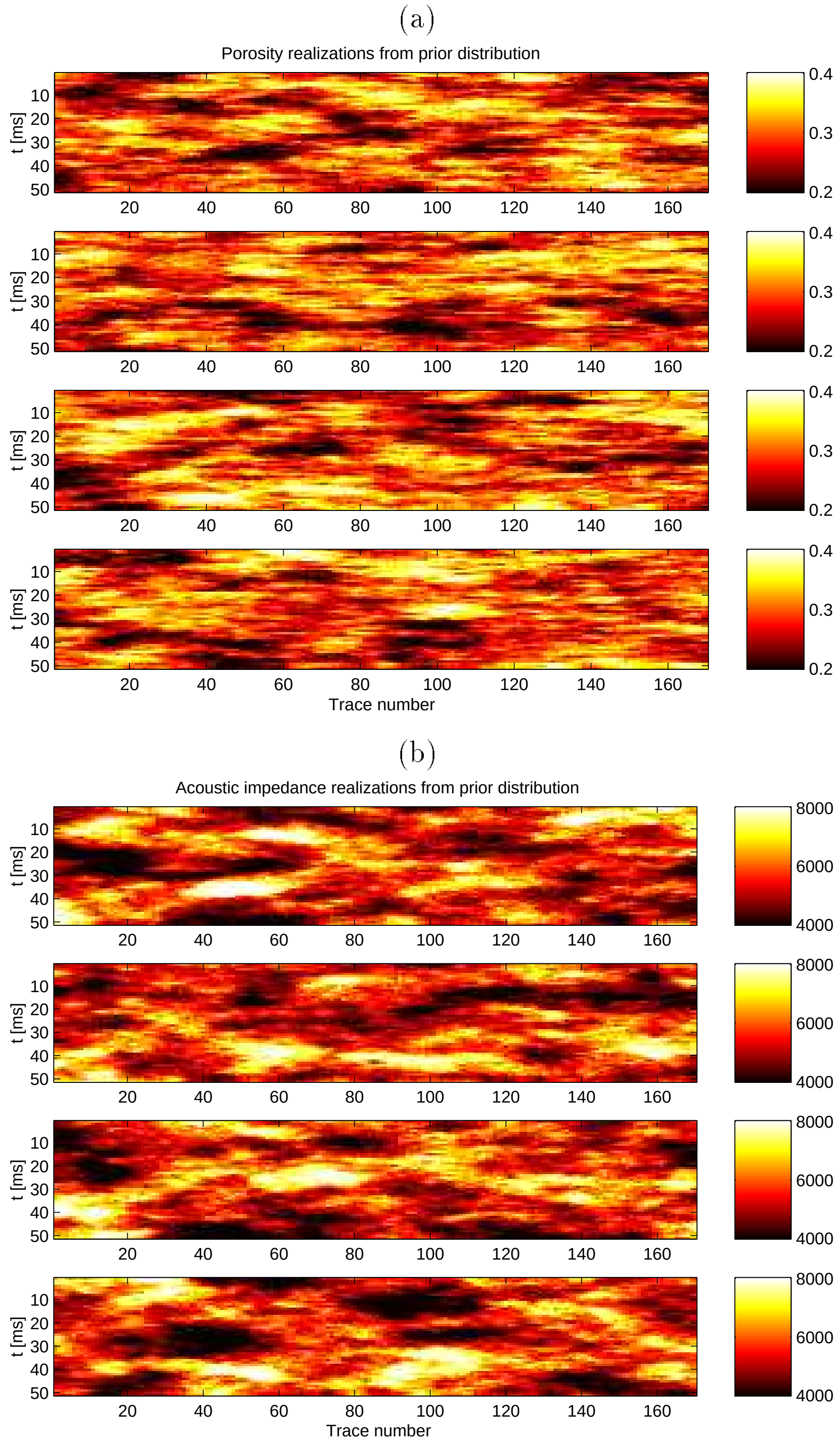

Figure 8: Samples from the prior pdf. (a) Porosity (b) Acoustic impedance.

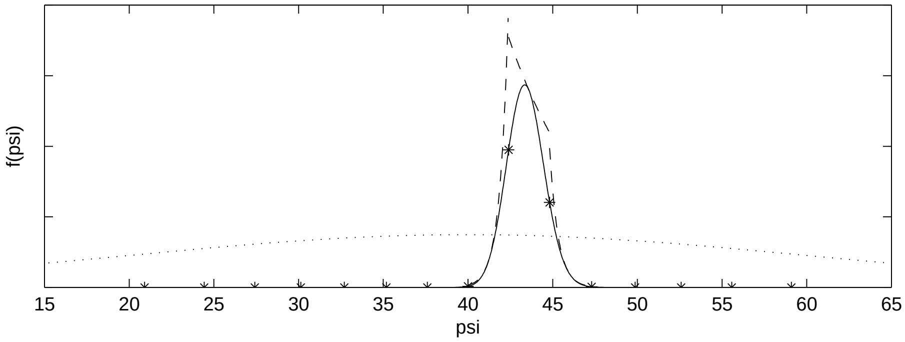

Figure 9: Pdf of seismic wavelet parameter (ψ). $\cdots$ prior; — posterior; $*$ interpolation points; $---$ envelope used in rejection sampling.

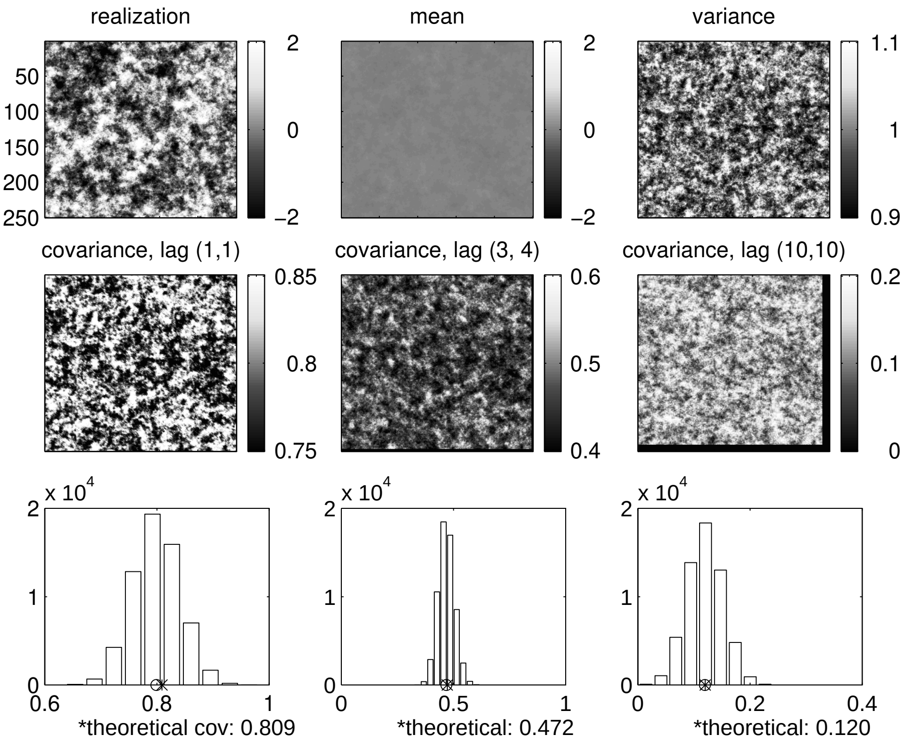

Figure 10: Summary of test results for the approximate algorithm for sampling from a Gaussian random field with extensive conditioning.

(a)

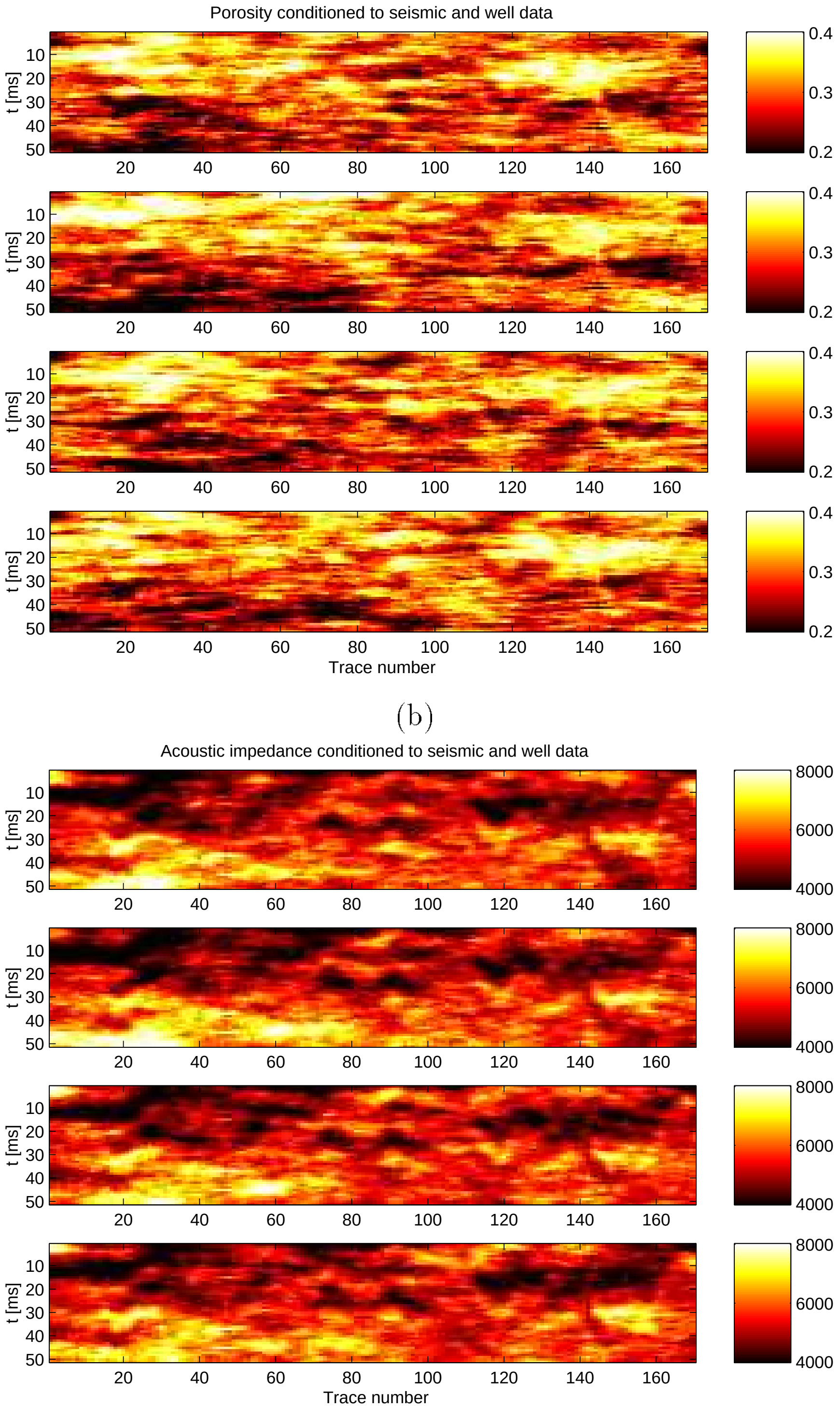

Figure 11: Samples from the posterior pdf. (a) Porosity (b) Acoustic impedance.

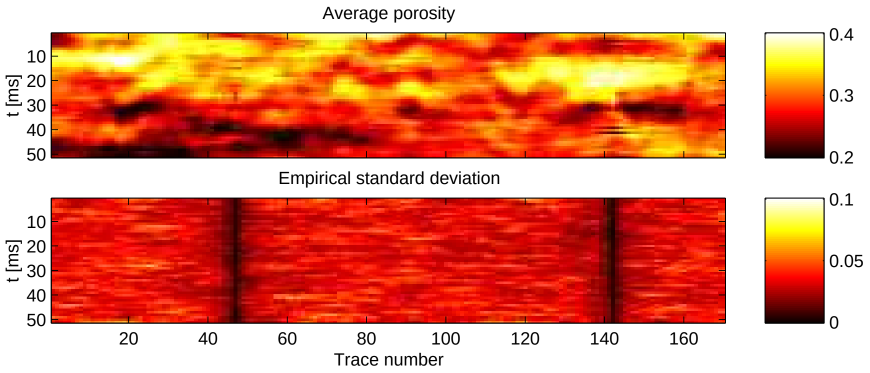

Figure 12: Average and empirical standard deviation of 10 samples of porosity from the posterior pdf.

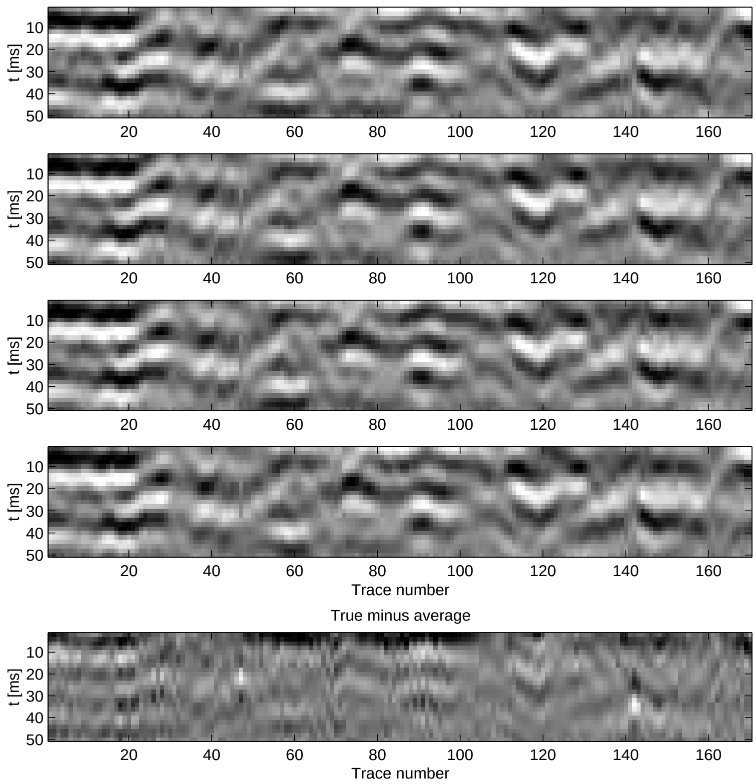

Figure 13: Simulated seismic amplitudes from 4 samples from posterior pdf. Deviation between observed and average of 10 simulations.

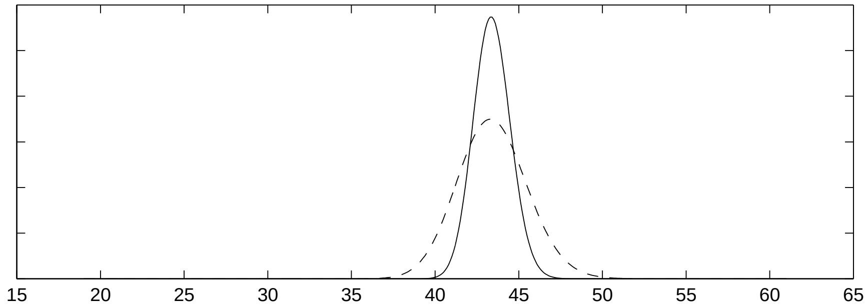

Figure 14: Posterior pdfs of seismic wavelet parameter (ψ). $---$ based on one trace per well only; — full spatial model.

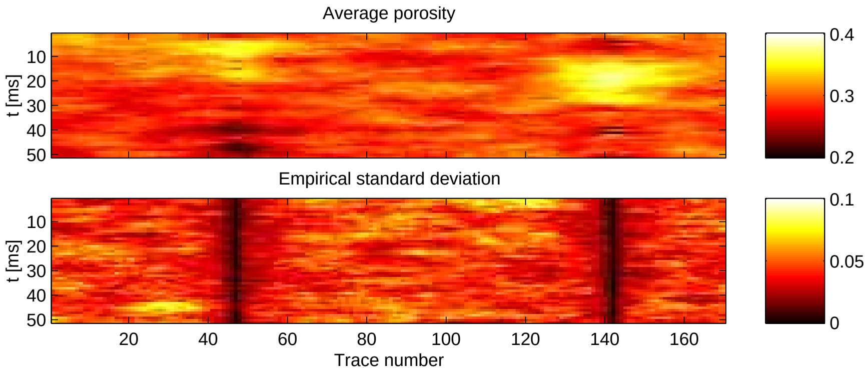

Figure 15: Average and empirical standard deviation of 10 samples of porosity conditioned on well observations only.